Orbitally forced hyperstratification of the Oligocene South Atlantic Ocean

Diederik Liebrand[1, 2, *], Isabella Raffi[3, *], Ángela Fraguas[4], Rémi Laxenaire[5], Joyce H. C. Bosmans[6], Frederik J. Hilgen[7], Paul A. Wilson[1], Sietske J. Batenburg[8], Helen M. Beddow[7], Steven M. Bohaty[1], Paul R. Bown[9], Anya J. Crocker[1, 10], Claire E. Huck[1], Lucas J. Lourens[7], Luciana Sabia[11]

*[1]National Oceanography Centre Southampton, University of Southampton, Southampton SO14 3ZH, UK; [2]MARUM - Center for Marine Environmental Science, University of Bremen, 28359, Bremen, Germany; [3]Dipartimento di Ingegneria e Geologia (InGeo), Università degli Studi "G. d'Annunzio" di Chieti–Pescara, 66013 Chieti Scalo, Italy; [4]Paleontology Department, University Complutense of Madrid, 28040 Madrid, Spain; [5]Laboratoire de Météorologie Dynamique, UMR 8539 École Polytechnique, ENS, CNRS, Paris, France; [6]Department of Physical Geography, Faculty of Geosciences, Utrecht University, 3508 TC Utrecht, The Netherlands; [7]Department of Earth Sciences, Faculty of Geosciences, Utrecht University, 3584 CS Utrecht, The Netherlands; [8]Department of Earth Sciences, University of Oxford, Oxford OX1 3AN, UK; [9]Department of Earth Sciences, University College London, Gower Street, London WC1E 6BT, UK; [10]Department of Animal and Plant Science, University of Sheffield, Sheffield S10 2TN, UK; [11]Department of Science and Technologies, University of Naples "Parthenope", 80143 Napoli, Italy; *These authors contributed equally to this study; Correspondence to: D. Liebrand (diederik@palaeoclimate.science), and/or I. Raffi (raffi@unich.it)*

This article has been accepted for publication and undergone full peer review but has not been through the copyediting, typesetting, pagination and proofreading process which may lead to differences between this version and the Version of Record. Please cite this article as doi: 10.1002/2017PA003222

Key Points

- Seven astronomically-forced open-ocean *Braarudosphaera* acmes occurred during the mid-Oligocene in the subtropical South Atlantic Ocean
- The exact paleoecologic, paleoceanographic, and paleoclimatic significance of the mid-Oligocene *Braarudosphaera* acmes remains unclear
- Recurrent hyperstratification can provide a virtual sea-floor, which may be required in *Braarudosphaera*'s life-cycle

Abstract

Pelagic sediments from the subtropical South Atlantic Ocean contain geographically extensive Oligocene ooze and chalk layers that consist almost entirely of the calcareous nannofossil *Braarudosphaera*. Poor recovery and the lack of precise dating of these horizons in previous studies has limited the understanding of the number of acmes, their timing and durations, and therefore their likely cause. Here we present a high-resolution, astronomically tuned stratigraphy of *Braarudosphaera* oozes (29.5–27.9 Ma) from Ocean Drilling Program Site 1264 in the southeastern Atlantic Ocean. We identify seven episodes with highly abundant *Braarudosphaera*. Four of these acme events coincide with maxima and three with minima in the ~110-ky and 405-ky paced eccentricity cycles. The longest lasting acme event corresponds to a pronounced minimum in the ~2.4-My eccentricity cycle. In the modern ocean, *Braarudosphaera* occurrences are limited to shallow marine and neritic settings, and the calcified tests of *Braarudosphaera* probably represent a resting stage in its life cycle. Therefore, we hypothesize that the Oligocene acmes point to extensive and episodic (hyper)stratified surface water conditions, i.e., a shallowly situated pycnocline that may have served as a virtual sea floor, which (partially) prevented the tests from sinking in the pelagic realm.

We speculate that hyperstratification was either ocean-basin-wide, through the formation of relatively hyposaline surface waters, or eddy-contained through strong isopycnals at the base of eddies. Astronomical forcing of atmospheric and/or oceanic circulation could have triggered these conditions through either sustained rainfall over the open ocean and adjacent land masses or increased Agulhas Leakage.

Index terms

0473 (Paleoclimatology and paleoceanography), 1125 (Chemical and biological geochronology), 4910 (Astronomical forcing), 4944 (Micropaleontology), 4950 (Paleoecology)

Keywords

Braarudosphaera acmes, astronomical forcing of atmospheric and oceanic fronts, surface-ocean stratification, Oligocene, monsoons, eddies

1. Introduction

The recovery of mid-Oligocene (~30–27 Ma) strata from the subtropical South Atlantic Ocean reveals geographically extensive ooze and chalk layers that are composed of the calcareous nannofossil *Braarudosphaera*. These *Braarudosphaera*-rich horizons are reported from Deep Sea Drilling Project (DSDP) Leg 3 [*Maxwell et al.*, 1970], Leg 40 [*Bolli et al.*, 1978], Leg 73 [*Hsü et al.*, 1984] and Leg 74 [*Moore et al.*, 1984], and more recently during Ocean Drilling Program (ODP) Leg 208 [*Zachos et al.*, 2004]. They are especially well-preserved on bathymetric highs on either side of the Tristan hotspot in areas above the lysocline, which currently lies at ~3800 m in the South Atlantic Ocean [*Boeckel and Baumann*, 2004]. At abyssal sites, such horizons are thinner or even absent, due to carbonate

dissolution below the lysocline [*Peleo-Alampay et al.*, 1999]. In the South Atlantic, the *Braarudosphaera* layers form a belt between ~20° and 30°S (Fig. 1) [*Noël and Melguen*, 1978; *Parker et al.*, 1985] that can be traced as a series of (weak) acoustic reflectors for thousands of kilometers across the basin [*Maxwell et al.*, 1970]. *Braarudosphaera*-rich sediments of mid-Oligocene age are also reported from other ocean basins, for instance at sites in the subtropical latitudes of the North Atlantic Ocean [*Parker et al.*, 1985] and the tropical and subtropical latitudes of the Indian Ocean [*Roth*, 1974; *Siesser et al.*, 1992]. However, the abundance of braarudosphaerids in the oozes from the South Atlantic, which are near-monospecific, is unequaled in other ocean basins [*Parker et al.*, 1985].

The Braarudosphaeraceae appeared in the earliest Cretaceous (ca. 140 Ma) and were particularly diverse and abundant in the Cretaceous and Paleogene [*Bown*, 2005a; *Gartner*, 1996; *Lamolda et al.*, 2005]. There are two extant species within the Braarudosphaeraceae and molecular phylogenetic studies place this family within the Class Prymnesiophyceae of the haptophyte eukaryotic algae [*Takano et al.*, 2006]. *Braarudosphaera bigelowii* is the best-known extant species and is found in neritic habitats, such as coastal/shelf settings and inland seas [*Bukry*, 1974; *Hagino*, 1997; *Konno et al.*, 2007; *Proto Decima et al.*, 1978; *Takayama*, 1972; *Tanaka*, 1991]. Enrichments of *Braarudosphaera* spp. in geological records have been linked to environmental conditions that mimic those of the neritic realm, such as shallow coastal waters with water depths $\lesssim$70 m ([*Martini*, 1967; *Takayama*, 1972; *Tanaka*, 1991] see also: [*Hagino et al.*, 2013]), hyposalinity [*Bukry*, 1974], eutrophism [*Bartol et al.*, 2008; *Cunha and Shimabukuro*, 1997; *Švábenická*, 1999] and/or perhaps a reduced water column transparency. In addition, *Braarudosphaera* spp. have been associated with climatologic and/or ecologic upheavals and interpreted to be opportunistic (r-strategist), and sporadic bloom-forming taxa that colonize challenging or vacant niches [*Bown*, 2005b; *Bukry*, 1974;

Minoletti et al., 2005]. The neritic ecology of *Braarudosphaera* spp. is unusual for calcifying prymnesiophytes (coccolithophores), which are more typically adapted to open ocean environments.

Three factors in particular have made the mid-Oligocene *Braarudosphaera* acmes an enigma: (*i*) the stark contrast between the restriction of modern *Braarudosphaera* to neritic settings, versus the presence of similar taxa in the pelagic realm during the mid-Oligocene (i.e., modern ecology versus paleoecology), (*ii*) the difference in surface ocean conditions of the modern South Atlantic Ocean (mixed, relatively hypersaline and oligotrophic) (Fig. 2) versus those that prevailed during mid-Oligocene (perhaps more stratified, hyposaline and eutrophic), which the *Braarudosphaera* acmes are thought to reflect (i.e., modern oceanography versus paleoceanography), and (*iii*) the unknown forcing-agents that can explain these ecologic and oceanographic contrasts between the present day and the geological past (i.e., modern climatology versus paleoclimatology) [*Kelly et al.*, 2003; *Peleo-Alampay et al.*, 1999]. One key aspect currently impeding understanding of the mid-Oligocene acmes is the absence of a detailed astrochronological framework for the *Braarudosphaera*-rich layers. Without a clear chronology, it is not possible to obtain an in-depth understanding of the cause-and-effect relationships between astronomical climate forcing and the resulting paleoceanographic/paleoecologic conditions that culminated in the *Braarudosphaera* acmes. Here, we present the first continuous and high-resolution stratigraphy across the *Braarudosphaera* oozes from subtropical South Atlantic Ocean ODP Sites 1264 and 1265, with the aim of investigating the number, duration, timing and recurrent nature of the acmes they represent.

2. Materials and methods

2.1. Site descriptions

Six sites were drilled along a depth transect on the Walvis Ridge during ODP Leg 208 (southeastern Atlantic Ocean) (Fig. 1). All but the two deepest sites recovered Oligocene *Braarudosphaera*-rich strata (Fig. 3) [*Zachos et al.*, 2004]. For this study we selected Sites 1264 (2505 meters below sea level (mbsl), ~2100 paleo-mbsl at 28.5 Ma, 28°31.955'S, 2°50.730'E) and 1265 (3059 mbsl, ~2550 paleo-mbsl at 28.5 Ma, 28°50.101'S, 2°38.354'E) that recovered relatively expanded, carbonate-rich Oligocene intervals (Fig. 1) [*Zachos et al.*, 2004]. The sediments are typical for a low-to-mid latitude pelagic setting and are dominated by biogenic carbonates that predominantly consist of calcareous nannofossil, with a smaller contribution of planktic and benthic foraminiferal remains and an almost complete absence of siliceous microfossils [*Zachos et al.*, 2004]. Magnetochron C11 was transposed from Site 1266 (3798 mbsl, ~3250 paleo-mbsl at 28.5 Ma, 28°32.550'S, 2°20.610'E) to Site 1264 using a detailed correlation between sites [*Bowles*, 2006; *Liebrand et al.*, 2016]. We made a small correction in the adjusted revised meters composite depth (armcd) for an off-splice interval of Core 1264B-29H, to better align it with the revised meters composite depth (rmcd) of the same interval identified on-splice in Core 1264A-29H. One mapping-pair for Core 1264B-29H (301.60 rmcd to 301.51 armcd) was replaced with two new mapping-pairs (302.06 rmcd to 301.46 armcd and 302.26 rmcd to 301.95 armcd). The composite depth model on the rmcd scale, the splice tie-points between Holes 1264A and 1264B, and the age model for Site 1264 remain unaltered from *Liebrand et al.*, [2016].

2.2. Sediment properties and stable isotopes

For stratigraphic and paleoceanographic context, we use previously published sediment property records (i.e., water content, $CaCO_3$ content, size fraction weights) and benthic foraminiferal stable oxygen ($\delta^{18}O$) and carbon ($\delta^{13}C$) isotope records [*Liebrand et al.*, 2011; *Liebrand et al.*, 2016], combined with newly generated bulk sediment $\delta^{18}O$ and $\delta^{13}C$ records and nannofossil abundance records. The $CaCO_3$ content was estimated from high-resolution x-ray fluorescence (XRF) core scanning data using the natural logarithm of calcium over iron counts, calibrated to shipboard coulometric $CaCO_3$ measurements ([*Zachos et al.*, 2004]; see [*Liebrand et al.*, 2016] for details). Bulk $\delta^{18}O$ and $\delta^{13}C$ isotope data were measured at ~5 cm resolution across the entire Site 1264 study interval (286–318 armcd) (Fig. 4). Bulk isotopes were measured at Utrecht University using a Thermo Finnigan GasBench-II carbonate preparation device coupled to a Thermo Finnigan Delta-V mass spectrometer. Analytical precision was 0.08 ‰ and 0.03‰ for $\delta^{18}O$ and $\delta^{13}C$, respectively. We applied a small (0.20 ‰) adjustment to the $\delta^{18}O$ data that was obtained on the Delta-V to match results of duplicate runs of a small sample-set that was measured using a Thermo Finnigan Kiel-III automated preparation system coupled to a Thermo Finnigan MAT 253 mass spectrometer, also at Utrecht University. The ratios for each sample were drift-corrected using nine isotopic standard (NBS-19) measurements analyzed within each run.

2.3. Calcareous nannofossils

Smear slides of bulk sediment were made using standard preparation techniques [*Bown and Young*, 1998], and were analyzed at Chieti University with a polarizing light microscope at 1250× magnification. Micrographs were taken with a scanning electron microscope (SEM) to visually assess coccolith/pentalith fragmentation, recrystallization and calcite overgrowth, and to aid species identification (Plate 1). Abundances of the holococcoliths of *Zygrhablithus*

bijugatus, nannoliths of *Discoaster* spp. (115 samples) and pentaliths of *Braarudosphaera* spp. (136 samples) were obtained by counting the number of specimens in a defined area of the smear slides (N/mm^2, counted in 30 fields of view in each sample) [*Backman and Shackleton*, 1983]. These counts provide a semi-quantitative measure of abundance because the number of specimens in each field of view varies amongst smear slides. Furthermore, quantifying *Braarudosphaera* spp. was not straightforward because the dodecahedral-shaped coccospheres consist of twelve pentaliths, which, in turn, are composed of five laminated, trapezoidal-shaped segments that easily disintegrate further into smaller fragments (Plate 1, images (B) and (C); [*Young et al.*, 2003]). The number of *Braarudosphaera* pentaliths was derived from counts of segments divided by five for most samples because complete pentaliths were preserved intact only in a few samples (Plate 1). These calculated abundances may represent an overestimate because of the potential further fragmentation of segments into the composite laminae. Also, the quality of the abundance records presented here may be compromised by the moderate-to-severe recrystallization, as seen in the SEM micrographs (Plate 1).

2.4. Tuned age model and time series analyses

All data, previously published and newly generated, are presented on a previously published, astronomically tuned age model (Fig. 5). This age model is based on the alignment of maxima in $CaCO_3$, interpreted to predominantly reflect productivity maxima, with 95 to 125-ky minima (i.e. ~110 ky) in the stable eccentricity solution [*Laskar et al.*, 2011; *Liebrand et al.*, 2016]. The *Braarudosphaera*-rich oozes were excluded during the tuning process because they distort the background cyclicity in $CaCO_3$, which is dominated by ~110-ky cycles. Higher frequency astronomical parameters were excluded from the tuning target-curve because of (*i*) the relatively weak expression of obliquity and precession signals in the Site

1264 records, (*ii*) the unknown phase relationship between $CaCO_3$ and precession [*Liebrand et al.*, 2016], and (*iii*) the uncertainty in the stability of the obliquity and precession solutions for ages ≳10 Ma [*Zeeden et al.*, 2014]. The eccentricity tuning is unaffected by these uncertainties and is precise and accurate at the ~110-ky level of tuning. To quantify the spectral power of the $CaCO_3$ record we used a multi-taper method [*Ghil et al.*, 2002], an evolutive Fast Fourier Transform, and Wavelet analysis (Fig. 6) [*Grinsted et al.*, 2004]. Gaussian filtering of the La2011_ecc3L nominal eccentricity solution and the *Braarudosphaera* pentalith record was applied to extract their 405-ky components (Fig. 7) [*Laskar et al.*, 2011; *Paillard et al.*, 1996].

3. Results

3.1. Stratigraphic records

We identify seven acmes of varying intensity in the combined lithologic, geochemical and *Braarudosphaera* spp. abundance records and we number these from old to young as "*Braarudosphaera* Acme Events" (BAE-1 to BAE-7) (Figs. 5 and 7). BAE-3 and BAE-5 are composed of multiple events of shorter duration, which are given a letter as appendix: BAE-3a, BAE-3b, BAE-5a, BAE-5b and BAE-5c. Core photographs reveal (Fig. 3) that BAE-3b and BAE-5b can be subdivided further into "couplet" or "triplet" horizons that probably reflect individual insolation peaks of relatively short duration (e.g., precession or obliquity maxima/southern hemisphere (SH) summer insolation maxima). Similar bundling of *Braarudosphaera*-rich layers has been observed in sediments recovered from DSDP Site 363 [*Kelly et al.*, 2003]. At Site 1264, BAE-7 is only partially recovered because of a short coring gap. Furthermore, the base of BAE-2 and the maxima of BAEs 3a and 5b overlap with core-section ends. These artifacts may have affected the quality of the data records in these specific intervals. However, the close agreement between the patterns observed in $CaCO_3$

from Sites 1264 and 1265 suggests that these issues are minor [*Liebrand et al.*, 2016]. The thicknesses of the BAEs as recorded in the $CaCO_3$ records from Sites 1264 and 1265 vary between ~10 and 35 cm (Fig. 4).

The sediment size-fraction records, combined with the high $CaCO_3$ values (~90–95 %) and smear-slide observations, strongly suggest that calcareous nannofossils make up the bulk of the sediments at Site 1264 (Fig. 4) [*Liebrand et al.*, 2016]. Over the *Braarudosphaera* oozes, the 0–38 μm size fraction increases from typical background values of ~95% to up to 98% of the dry sample weights. The *Braarudosphaera*-rich samples were difficult to wash over a sieve and size-fraction weights across these oozes may be affected by poor disintegration of the more lithified sediments, resulting in lower weights for the smaller size-fractions and higher weights for the greater size-fractions. Similar difficulties have been reported for *Braarudosphaera*-rich samples from DSDP Site 362 [*Diester-Haass*, 1988]. The water content of the sediment (expressed as percentages of the total wet-sample weights) decreases sharply from ~25% to 15% across the six most prominent *Braarudosphaera* oozes. This probably reflects lower porosity of the bulk sediment resulting from a smaller contribution of foraminifera (Fig. 4). Absolute values in the $CaCO_3$ records agree well between Sites 1264 and 1265 and generally vary around ~92% $CaCO_3$ of dry sample weight, but increase to nearly 100% $CaCO_3$ in the *Braarudosphaera*-rich layers.

The benthic $\delta^{18}O$ and $\delta^{13}C$ stratigraphies are characterized by a ~1.0‰ amplitude variability on eccentricity timescales, and the ~110- and 405-ky cycles are particularly well expressed in the benthic $\delta^{18}O$ and $\delta^{13}C$ series, respectively [*Liebrand et al.*, 2016]. These large amplitude ~110-ky cycles in benthic $\delta^{18}O$ are interpreted to reflect substantial waxing and waning of the Antarctic ice sheets, with the largest glacial maxima reaching sizes equivalent to

approximately 85–110% of the modern ice volume on East Antarctica [*Liebrand et al.*, 2017]. The bulk $\delta^{18}O$ record shows six prominent positive excursions from background values of ~1.5‰ to peak values of ~2.5 to 3.0‰ concurrent with BAEs 3a, 3b, 5a, 5b, 6, and 7. Similar isotopic shifts across *Braarudosphaera* oozes have previously been noted in bulk records from the South Atlantic and Indian Ocean [*Kelly et al.*, 2003; *Peleo-Alampay et al.*, 1999; *Siesser et al.*, 1992]. The absence of strong bulk $\delta^{18}O$ excursions during BAEs 1, 2, and 4 is suggestive of a smaller contribution of *Braarudosphaera* to the bulk sediment. The largest fluctuations in the bulk $\delta^{18}O$ record can be explained by disequilibrium "vital effects" and/or preferential sea floor diagenetic alteration of bulk calcite $\delta^{18}O$ in the BAEs. The exact biochemical mechanisms causing strong isotopic fractionation are currently unknown because culturing of *B. bigelowii* has not been successful to date [*Hagino et al.*, 2013; *Hagino et al.*, 2016], but it is a common feature seen in coccolithophores [*Bolton et al.*, 2012; *Hermoso et al.*, 2014; *Stoll and Ziveri*, 2004]. However, diagenesis could explain the entire increase in bulk carbonate $\delta^{18}O$ towards higher values, because both bulk and benthic $\delta^{18}O$ values reach maximum values of ~2.5 to 3.0‰ after the benthic values are adjusted to equilibrium calcite (note that uncorrected values are depicted in Figs 4 and 5) [*Bukry*, 1981]. The bulk $\delta^{13}C$ record varies between 1.5 and 2.5‰ and shows no similarly prominent excursions during the mid-Oligocene (Figs. 4 and 5).

3.2. Age model and time series analysis

The BAEs at Site 1264 occur within a 1.6-My time interval that spans from 29.5 to 27.9 Ma, on the eccentricity-tuned age model [*Liebrand et al.*, 2016]. The acmes are concurrent with 405-ky eccentricity Cycles 73–69 of the Rupelian (early Oligocene) and Chattian (late Oligocene) stages of the 2012 Geologic Time Scale (GTS2012, [*Vandenberghe et al.*, 2012]). The Oligocene nannofossil biohorizons Base (i.e., lowest or first occurrence) *Sphenolithus*

distentus (315.14 armcd) and Base *Sphenolithus ciperoensis* (289.66 armcd) have been identified in the studied interval (Fig. 4) and are astronomically dated at ~29.81 and ~27.02 Ma, respectively (Fig. 5). The tuned ages for these bioevents at Site 1264 are 190 and 120 ky younger, respectively, than the calibrated ages in the most recent Paleogene nannofossil biochronology (i.e., 30.00 and 27.14 Ma, respectively; [*Agnini et al.*, 2014]). A direct comparison to the GTS2012, which for the Oligocene Epoch follows the manually tuned ages for equatorial Pacific ODP Site 1218 [*Pälike et al.*, 2006] indicates that all BAEs identified at Sites 1264 and 1265 fall within magnetochrons C10n.1n–C11n.1r [*Liebrand et al.*, 2016; *Vandenberghe et al.*, 2012]. This finding is supported by the only reliable reversal identified at Site 1266, namely the top of Chron C11n, which is transferred to Site 1264. The independently tuned age for this reversal is in excellent agreement with the tuned Site 1218 age and the GTS2012 [*Liebrand et al.*, 2016; *Pälike et al.*, 2006; *Vandenberghe et al.*, 2012].

Time-evolutive spectral analysis of the $CaCO_3$ record from Site 1264 show that high spectral power is present in a frequency range of ~10.0–25.0 cycles/My, which corresponds to periodicities of ~110–40 ky/cycle (Fig. 6A). Weaker spectral peaks can be identified at the ~2.5, ~5.0 and ~32.0 cycles/My frequencies, i.e., the ~405-, ~200- and ~31-ky periodicities. In contrast, wavelet analysis on the $CaCO_3$ record from Site 1264 reveals significant spectral power near the precession frequencies (Fig. 6B) [*Liebrand et al.*, 2016]. A filter of the 405-ky periodicity present within the *Braarudosphaera* spp. abundance record shows a very strong response during the ~2.4-My eccentricity minimum at ~28.5 Ma. During ~2.4-My minima, the 405-kyr component of eccentricity is most strongly expressed and this appears to be highly amplified in the abundance record.

3.3. Calcareous nannofossil abundance, taxonomy and species concepts

Variability in the amplitude of the BAEs is apparent in the *Braarudosphaera* spp. abundance record, and, apart from peak values during BAE-5 (~490/mm^2), a general trend of increasing amplitude is observed through the succession of *Braarudosphaera* oozes (BAE-1 ~140 N/mm^2 to BAE-7 ~370 N/mm^2) (Figs. 4 and 5). The *Braarudosphaera* abundance record generally confirms the number of BAEs observed in the $CaCO_3$ and bulk $\delta^{18}O$ records. It also shows that not all of the acmes were of the same magnitude, and that some lack a clear lithological/geochemical expression. Both *Discoaster* spp. and *Z. bijugatus* are strongly anticorrelated with *Braarudosphaera* spp. abundance (Fig. 5). These patterns suggest that *Braarudosphaera* spp. outcompeted and/or diluted *Z. bijugatus* and *Discoaster* spp. during the acmes.

The SEM images show *Braarudosphaera* and *Discoaster* specimens were more adversely affected by recrystallization and calcite overgrowth than other nannofossil taxa, and for many *Discoaster* specimens the overgrowth was so severe that an unambiguous visual identification to species level was not possible (Plate 1). However, very few *Discoaster* species are present in the Oligocene [*Bukry,* 1978b] and it is likely that the dominant six-rayed discoasterids are *Discoaster deflandrei* and scarce five-rayed specimens are *Discoaster tanii*. The abundance record combines all *Discoaster* species encountered and we refer to these as *Discoaster* spp. Similarly, identification of *Braarudosphaera* specimens remained ambiguous. The Oligocene specimens appear too large to belong to the extant species *B. bigelowii*, and resemble the extinct species *B. perampla* [*Bown*, 2010; *Raffi et al.*, 2016]. We therefore refer to these Oligocene *Braarudosphaera* specimens as *Braarudosphaera* spp., but they are most probably extinct close-relatives of the living *B. bigelowii* species-complex.

4. Astrochronology

4.1. Durations of the acmes

The eccentricity-tuned age model for Site 1264 is constructed using linearly interpolated ages between tuning tie-points every ~125 ky [*Liebrand et al.*, 2016]. To obtain approximate durations of the BAEs, we assume that the effect of bioturbation was limited ~10 cm vertically. During deposition of the *Braarudosphaera* oozes, sedimentation rates likely increased sharply, complicating the estimation of their duration. Despite these uncertainties, we find that the BAEs at Site 1264 show large variability in durations (Table 1). BAE-3 and BAE-5 both consist of several closely spaced, hence shorter-lasting, acmes, which combined have durations of ~160 and ~210 ky, respectively (Table 1). BAE-5, which has the longest duration and highest amplitude, thus persisted for the greater part of 405-ky Eccentricity Cycle 71 (Figs. 5 and 7). The acmes identified in the *Braarudosphaera* abundance record (i.e., BAEs 1, 2, 3a, 3b, 4, 5a, 5b, 5c, 6, and 7) have durations ranging from ~20 to 80 ky (~55 ky on average). These durations broadly correspond to the insolation periodicities and may represent single or multiple precession or obliquity cycles. Superimposed on BAE-3b and BAE-5b, three relatively brief events (~20 ky each, not numbered) are identified (Figs. 3 to 5, Table 1). These relatively short-lived events are expressed in the lithological record as individual ooze layers and are probably paced by the precession cycle (Fig. 3). Lithologically similar *Braarudosphaera* layers from DSDP Site 363 were estimated to have been deposited over a period of 1 to 2 ky each, based on a linear interpolation between magnetostratigraphic reversal ages [*Kelly et al.*, 2003]. These very short durations contrast with the estimates based on the record from Site 1264, which suggest that (*i*) deposition of individual *Braarudosphaera* oozes lasted up to a (phase of a) 20-ky precession cycle (or 40-ky obliquity cycle), and (*ii*) the entire BAE-5 had a duration of >210 ky.

4.2. Astronomical pacing of the acmes

The *Braarudosphaera* event with the longest duration on the eccentricity-tuned age model is BAE-5, and it is contemporaneous with a very pronounced minimum in the ~2.4-My eccentricity cycle at ~28.5 Ma, which coincides with the high amplitude 405-ky Eccentricity Cycle 71 that is characterized by low amplitude ~110-ky cycles (Fig. 5) [*Liebrand et al.*, 2016]. A strong expression of the ~405-ky beat is present in the *Braarudosphaera* abundance record (Fig. 7). BAEs 2, 3, and 6 concur with ~110-kyr eccentricity maxima which, apart from during BAE-2, have a relatively subdued amplitude because of the ~2.4-My eccentricity minimum. However, BAE-1 (weak), BAE-4 (weak), and BAE-7 (strong) are concurrent with ~110-ky eccentricity minima. The opposite phase relationships between most BAEs and different eccentricity periodicities (i.e., they are concurrent with a ~2.4 My eccentricity minimum, and most BAEs also with 405- and ~110 ky eccentricity maxima) indicate a complex forcing mechanism. Three lines of evidence suggest that obliquity and precession cycles paced the BAEs, despite the uncertainty in the exact phase relationships. First, BAEs 2, 3, 5 and 6 occur during 405-ky eccentricity maxima (Fig. 7), suggesting a pacing of these acmes by (eccentricity-modulated) precession. Second, two of the acmes (BAE-3b and BAE-5b) each comprise multiple prominent *Braarudosphaera*-rich layers that are separated by brief intervals of lower *Braarudosphaera* abundance (Figs. 3 to 5). This is indicative of a bundling of lithological cycles and probably reflects groups of precession-paced events (Table 1). Third, the $CaCO_3$ record across the *Braarudosphaera* acmes contains the highest-frequency spectral power associated with the obliquity and precession cycles according to the evolutive and wavelet analyses, respectively (Fig. 6). Both the precession- and obliquity-dominated pacing of the acmes is in agreement with independent estimates for inter-bed periods of 100 ky or less for the *Braarudosphaera*-rich layers recorded at Site 362 [*Bukry*,

1978a]. No clear relationship is observed between ~175-ky amplitude modulations of obliquity and the acmes, despite strong spectral power near a ~200-ky periodicity (Fig. 5).

5. Discussion

The high-resolution records from Sites 1264 and 1265 convincingly show, for the first time, that astronomical climate forcing was a key contributing factor to the formation of the South Atlantic *Braarudosphaera* acmes. Yet, the exact paleoecologic, paleoceanographic and paleoclimatologic significance of the BAEs remains elusive because of the poor constraints on the life cycle of this group of calcareous nannoplankton. In this discussion, we will briefly summarize the current understanding of the life cycle of the extant species *B. bigelowii*, and subsequently speculate on two mechanisms that can link astronomical forcing to aberrant, climatologic and oceanographic conditions potentially conducive to *Braarudosphaera* calcification.

5.1. The life cycle of *B. bigelowii*

To date, the extant *B. bigelowii* has not been cultured successfully, nor has its life cycle been directly observed, and its exact ecologic preferences thus remain unclear [*Hagino et al.*, 2013; *Hagino et al.*, 2016]. Yet, two observations provide some constraints on *B. bigelowii*, namely: (*i*) this taxon most probably has alternating life cycle stages that correspond to the number of chromosomes in the cell: one stage is motile, non-calcifying and probably haploid; the other is non-motile, calcifying and probably diploid [*Billard and Inouye*, 2004; *Hagino et al.*, 2013; *Thompson et al.*, 2012], and (*ii*) the species belonging to the genus *Braarudosphaera* have no test perforations and thus likely reflect a (non-reproductive) resting stage or "cyst" [*Billard and Inouye*, 2004]. If we accept these constraints on *Braarudosphaera*'s life cycle and combine this information with the modern day

biogeographical distribution, which shows that *B. bigelowii* is limited to neritic settings that are generally characterized by shallow water depths [*Martini*, 1967; *Takayama*, 1972; *Tanaka*, 1991], we can tentatively infer that *Braarudosphaera* spp. may require a sea-floor during its non-motile, calcifying resting stage, that prevents the cysts from sinking. Similar to previous authors, we speculate that the mid-Oligocene acmes may indicate phases of decreased reproduction, increased encystment, and perhaps increased unfavorable paleoecologic conditions for *Braarudosphaera* to thrive in its motile non-calcifying stage [*Bown*, 2005b; *Bukry*, 1978a; *Bybell and Gartner*, 1972; *Fischer et al.*, 1967].

5.2. Towards a mechanistic understanding of the Oligocene acmes

Two observations are key to unraveling the main causes of the mid-Oligocene BAEs. First, the most geographically extensive occurrences of *Braarudosphaera* are in both the North and the South Atlantic, broadly around 30°N and 30°S, respectively (Fig. 8) [*Parker et al.*, 1985]. Second, the oozes from Sites 1264 and 1265 are astronomically paced (Figs. 5 to 7 and Table 1). We argue that these observations, i.e., the biogeography and timing of events, can be explained by astronomical forcing of the mid-Oligocene climate system and the responses of the atmosphere and surface ocean. We propose two different chains of events capable of linking astronomical forcing of the climate system (part 1, shared by both hypotheses), to latitudinal migrations of atmospheric and/or oceanic fronts [*Bard and Rickaby*, 2009; *Bosmans et al.*, 2015b; *Peeters et al.*, 2004] and pycnocline and/or thermocline shallowing, hyperstratification and recurrent *Braarudosphaera* acmes in the South Atlantic Ocean (part 3, also shared by both hypotheses). The first mechanism (i.e., the Monsoon Hypothesis; part 2a) proposes basin-wide hyperstratification through increased moisture transport to the South Atlantic Ocean; the second mechanism (i.e., the Eddy Hypothesis; part 2b) proposes eddy-

contained hyperstratification through strong isopycnals at the base of the eddies and increased eddy formation by either the proto-Benguela Current, Agulhas leakage, or both.

(1) Insolation forcing of the BAEs

The concurrence of the best-developed acmes with a very pronounced minimum in the ~2.4-My eccentricity cycle (Figs. 5 and 7), suggests that the oceanographic mechanism that facilitated the BAEs was enhanced as a result of the prolonged absence of insolation "extremes" at the low-to-mid southern latitudes. In this interpretation the anomalous occurrence of BAEs 2 and 6 with ~110-ky eccentricity maxima is explained by interference between obliquity and precession that operated to cancel out their effects on low-to-mid southern latitude insolation. Such interference, during (at least) these two events, brings all BAEs in agreement with a hypothetical regional insolation-threshold (Fig. 7), below which conditions were suitable for acmes to develop. Yet, we cannot be certain about interference between obliquity and precession at these times because the astronomical solution for these parameters is not stable for ages >10 Ma [*Zeeden et al.*, 2014].

(2a) Monsoon Hypothesis: Atmospheric circulation and the hydrological cycle

We propose that sustained wet monsoon conditions increased the annually averaged oceanic rainfall over the subtropical South Atlantic Ocean and caused a reduction of surface-ocean salinity [*Bukry,* 1974]. This hypothesis is based on the concurrence of the BAEs with a ~2.4-My eccentricity minimum, when the amplitude of precession is reduced. We assume that dry and/or stormy winter monsoons were limiting *Braarudosphaera* acmes during times with relatively higher amplitude precession cycles (i.e., ~2.4-My eccentricity maxima), through insufficient build-up of relatively

"fresher" surface waters and/or through too much surface ocean mixing, respectively. The hypothesized sustained wet monsoon conditions, during the ~2.4-My eccentricity minimum, were amplified on astronomical time scales during more favorable precession and obliquity paced insolation conditions. Increases in oceanic rainfall at ~30°S could have been caused by a weakening of the Hadley Circulation (Fig. 8), for example, or by a very significant southward shift of the low pressure systems that are generally associated with the intertropical convergence zone (ITCZ; see published modeling examples that use present day geography: Fig. 9A–B).

(2b) Eddy Hypothesis: Atmospheric circulation and eddy formation

In this alternative hypothesis, we propose that increased eddy formation was caused by intensification of the proto-Benguela Current through the strengthening of the Easterlies, or by increased Agulhas leakage due to the southward migration of the SH subtropical (oceanic) front [*Bard and Rickaby*, 2009; *Peeters et al.*, 2004]. Similarly to the mechanism proposed in the Monsoon Hypothesis, one phase of the precession cycle must have prevented enhanced eddy formation in earlier and later time periods when the amplitude of eccentricity was greater.

We speculate that warm SH summers during high-amplitude eccentricity-modulated precession cycles weakened the Easterlies and reduced the formation of proto-Benguela upwelling eddies (both cyclonic and anticyclonic). Alternatively, cold SH winters during these orbits, moved the subtropical front northwards too much for sufficient Agulhas rings (predominantly anticyclonic) to enter and cross the South Atlantic Ocean.

(3) Hyperstratification and Braarudosphaera acmes

Following the Monsoon Hypothesis, we propose that the cumulative build-up of fresher (i.e. relatively hyposaline) surface waters during a prolonged interval of wetter winters in combination with reduced winter mixing caused the build-up of a lower-salinity surface water lens, as is depicted in Fig. 1. In contrast, following the Eddy Hypothesis, increased proto-Benguela upwelling eddies and/or Agulhas leakage changed the physicochemical properties of the South Atlantic surface ocean. In this hypothesis, consecutive summers (though not of maximum amplitude) during the ~2.4-My eccentricity minimum, in combination with a sufficient shedding of eddies during the relatively weak winters caused the more frequent traversing of eddy-contained surface waters across the basin (Fig. 9C). The proposed mechanisms of both the Monsoon and Eddy hypotheses could have resulted in a relatively shallow pycnocline or thermocline and regional (ocean-basin-wide) or localized (eddy-contained) salinity/temperature stratification of the surface ocean – conditions we refer to as "hyperstratification" [*Reichart et al.*, 2004]. This regional or local shallowly situated pycno-/thermocline could have served as a virtual sea floor [*Reichart et al.*, 2004] capable of concentrating *Braarudosphaera* in the water column.

These chains of events are distinct from that previously proposed for hyperstratified conditions in the northern Arabian Sea, during the Pleistocene [*Reichart et al.*, 2004]. There, the formation of a highly saline mixed layer and a strong density gradient followed glacial overturning events (i.e., Heinrich events). Such a mechanism was invoked to explain the presence of a lagoonal dinoflagellate species in the open ocean, and the hyperstratified conditions were postulated to simulate a shallow seafloor that is needed for the germination

of the dinoflagellate cysts [*Reichart et al.*, 2004]. A similar link to glacial overturning events for hyperstratification of the Oligocene South Atlantic Ocean is unlikely because we do not find a strong correlation between benthic $\delta^{18}O$ values and the BAEs (Figs. 4 and 5).

5.3. Atmospheric circulation

If we accept astronomically forced changes in hydroclimate as the forcing factor responsible for the BAEs (i.e. the Monsoon Hypothesis), then we need to identify the atmospheric circulation changes that could have caused the monsoonally driven increases in rainfall over the surface ocean (and adjacent continents) needed for hyperstratification. Potential mechanisms include: (*i*) a weakening of the Hadley circulation causing a slowdown of moisture transport away from the subtropical high-pressure belt, where relatively cold and dry air of the Hadley and Ferrel cells sinks underneath the flow of the subtropical jet (Fig. 8), and (*ii*) a significant southward migration of the intertropical convergence zone (ITCZ) and associated low-pressure system, where warm and wet air of the Hadley cells rises (Fig. 8). Both of these mechanisms could increase the freshwater budget in the subtropical South Atlantic Ocean.

Support for a sustained southwards shift of low air-pressure systems can be found in climate modeling studies of the Pleistocene (Fig. 9). Computed precipitation anomalies between precession minima and maxima, using an atmospheric circulation model and present-day geography, show that precession forcing exerts the strongest control on the redistribution of moisture at low-to-mid latitudes by modulating the amplitude of seasonal monsoons (Fig. 9A) [*Bosmans et al.*, 2015b; *Mohtadi et al.*, 2016]. In addition, this model supports a smaller contribution of obliquity forcing to monsoon intensity [*Bosmans et al.*, 2015a]. A different modeling study, comparing moisture transport between the Last Glacial Maximum and

Heinrich Stadial 1, using modern day geography and including changes in radiative forcing (i.e., isolation and greenhouse gasses), shows an increase in rainfall over the South Atlantic Ocean at tropical to subtropical latitudes between these two time periods (Fig. 9B) [*Liu et al.*, 2009; *Mohtadi et al.*, 2016; *Otto-Bliesner et al.*, 2014]. These two studies of the Pleistocene are driven by different mechanisms than the one we propose for the Oligocene. However, they show that a basin-wide rain belt can develop and persist on astronomical time scales over the South Atlantic Ocean along a ~10°S latitudinal band.

No similar modeling has been performed for the mid-Oligocene time interval, but given these modeling examples for the Pleistocene we deem larger changes in hydroclimate during the Oligocene a possibility, especially considering the different paleoclimatic and paleogeographic boundary conditions. The ITCZ in the Pacific is suggested to have migrated northwards in response to extra-tropical cooling associated with Antarctic glaciation across the Eocene-Oligocene transition [*Hyeong et al.*, 2016]. But a much greater latitudinal shift in the ITCZ of the opposite sign (southwards) is required to explain the mid-Oligocene BAEs through overhead precipitation. This observation raises feasibility questions from the perspective of atmospheric heat transport [*Donohoe et al.*, 2013] and perhaps points to the importance of freshwater delivery by large African and South American rivers systems with headwaters in lower latitudes. Regardless, from a physical oceanographic perspective, it is hard to conceive a stagnant South Atlantic surface ocean to persist for long periods of time (e.g. several months per year, annually recurring for thousands of years), thought to be needed for the BAEs to occur and form laminated (at Site 20 at least), laterally extensive, decimeter-thick ooze packages. The absence of organic rich sediments in the South Atlantic during the mid-Oligocene indicates that bottom waters remained well oxygenated throughout the BAEs, and that stratification must thus have been a surface-ocean phenomenon.

5.4. Dynamics at the oceanic mesoscale

Eddies in the modern ocean are characterized by complex and dynamic behavior, including "eddy trapping" and "eddy pumping" [*McGillicuddy Jr.*, 2016]. Eddy trapping refers to the pinching off of fluid rings (approx. 40-280 km in diameter, with cores of ~50 km [*Wang et al.*, 2015] and life times of a few days to two years) that can transport associated planktonic ecosystems inside them from, for example, the Indian Ocean into the South Atlantic Ocean [*Villar et al.*, 2015]. In the modern, both the Benguela Current and the Agulhas retroflection produce rings (eddies) that can propagate far into the interior of the South Atlantic Ocean and thereby provide lateral fluxes of physical, chemical and biological properties (Fig. 9C) [*Lehahn et al.*, 2011; *McGillicuddy Jr.*, 2016; *Villar et al.*, 2015]. Many of the modern Agulhas retroflection-derived eddies have at least ~30% of their contents derived from the Indian Ocean and are found to travel across the subtropical gyre, before disintegrating [*Wang et al.*, 2015]. Eddy pumping is the dynamic process of upwelling or downwelling within cyclonic (SH clockwise) and anticyclonic (SH anticlockwise) eddies that dome or depress the seasonal and mean pycnoclines, respectively [*McGillicuddy Jr.*, 2016]. For cyclonic eddies this results in density surfaces that coincide with the base of the euphotic zone (~500 m water depth), which could constitute the virtual seafloor potentially important for *Braarudosphaera* during its resting stage.

We speculate that a greater number of proto-Benguela Current-derived eddies, or rings shedding from the Agulhas retroflection, resulted from astronomically forced intensifications of the Easterlies, or a southward shift of the (oceanic) subtropical front, respectively. These chains of events may provide an explanation for the increase in calcification and export productivity associated with the BAEs, in an otherwise oligotrophic central gyre. However, the near-monospecific nature of the *Braarudosphaera* oozes is difficult to explain if eddy

occurrence alternated with gyre conditions that were host to normal planktonic populations. Another potential problem with the Eddy Hypothesis could be the gradual subduction of eddies, in the present day, to ~600 m water depth upon leaving the Cape Basin (Fig. 9C) [*Arhan et al.*, 1999; *Garzoli et al.*, 1999; *Herbette et al.*, 2004]. Subduction would not necessarily limit the habitable environment for *Braarudosphaera* to the eastern South Atlantic, because similar to the base of eddies, the boundary between the tops of the subducted eddies and the overlying surface waters are characterized by a strong pycnocline and thermocline [*Pegliasco et al.*, 2015], and could potentially serve as a physical barrier that partially prevents biota from sinking.

The Eddy Hypothesis does not explain why *Braarudosphaera* are not found in earlier and later episodes with similar, but hypothesized, weaker, dynamics at the oceanic mesoscale in the South Atlantic. However, the geographic overlap between the modern day Benguela eddy and Agulhas ring corridors, and the Oligocene *Braarudosphaera* belt is striking (Fig. 9C) [*Chelton et al.*, 2011; *Pegliasco et al.*, 2015], despite poor constraints on the exact latitudinal extent of the South Atlantic *Braarudosphaera* belt due to a scarcity of drill sites between ~0° and 25° S and between 35° and 50° S (Fig. 1) [*Peleo-Alampay et al.*, 1999]. Nevertheless, acoustic horizons linked to *Braarudosphaera* oozes can be traced to Site 360 in the southern Cape Basin (near Cape Town, [*Bolli et al.*, 1978]), making the geographic match even more compelling. The greater contribution of *Braarudosphaera* fragments to the bulk sediment in the South Atlantic compared to the North Atlantic matches the greater longevity of eddies in the former basin [*Chelton et al.*, 2011].

5.5. Recurrence of the acmes

The records from Sites 1264 and 1265 show that the BAEs were recurrent on eccentricity to precession time scales, and were sustained phenomena that persisted for several thousand up to hundreds of thousands of years. Next to this evidence for astronomical forcing of the Oligocene BAEs through the latitudinal migrations of atmospheric fronts, a couple of observations shed further light on climatic/oceanographic mechanisms. First, greater numbers of acmes are described at sites near the continental margins than at pelagic sites (e.g., at least 34 cyclical *Braarudosphaera* oozes at Site 362 [*Bukry*, 1978a]). Second, the best-developed ooze at Site 20, located in the western part of the South Atlantic Ocean, shows laminae (Fig. 1) [*Maxwell et al.*, 1970].

In the Monsoon Hypothesis, the greater number of acmes in drill cores from the African continental margin suggests that these surface waters were more frequently stratified than those overlying open ocean sites. We speculate that the ~34 layers at Site 363 reflect precession-paced run-off events, similar in origin perhaps to the precession-paced sapropels of the Miocene-Pleistocene Mediterranean. Hyperstratification (and sapropel formation) of the Mediterranean occurred more readily due to the greater influx of freshwater during the wet summer monsoon, both from increased runoff and directly through oceanic rainfall [*Bosmans et al.*, 2015b; *Bosmans et al.*, 2015c]. The laminae at Site 20 suggest that individual BAEs consist of annual layers that could reflect a seasonal amplification of the sustained moderately wet monsoon conditions that were already prevailing throughout the year. The laminae represent recurring blooms of *Braarudosphaera* that probably coincided with the annual wet summer monsoons.

In the Eddy Hypothesis, the greater number of BAEs preserved at Site 362 and 363 would reflect a greater number and more continuous stream of eddies and/or Agulhas rings forming and passing over this region of the subtropical South Atlantic, despite the fact that the Benguela Current, responsible for many eddies in this region in the modern, did not develop or fully intensify until the middle Miocene [*Diester-Haass*, 1988; *Diester-Haass et al.*, 1990], and that, present-day Agulhas rings do not travel so far to the North-East (Fig. 9C). The laminae found at Site 20 would in this hypothesis reflect productivity increases associated with eddies moving overhead, alternated with relative brief intervals of no deposition, until the next *Braarudosphaera*-laden eddy arrived.

5.6. Oligocene climatic boundary conditions

The *Braarudosphaera* oozes at Sites 1264 and 1265 are restricted to a 1.6-My interval (~29.5 to 27.9 Ma) and have not yet been identified during earlier and later ~2.4-My eccentricity minima. This suggests that other boundary conditions than astronomical configurations, such as climate evolution during the mid-Oligocene, caused the South Atlantic basin to become sensitive to seasonal hyperstratification under favorable insolation conditions. Long-term climate evolution during the Oligocene is characterized by a cooling trend/Antarctic ice sheet expansion during the early Oligocene (~33.9 to 28.0 Ma), a generally cold mid-Oligocene glacial interval (~28.0 to 26.3 Ma) that is characterized by a generally large, but highly unstable, Antarctic ice sheet, and a late Oligocene phase of global warming/reduction in Antarctic ice volume (~26.3 to 23.7 Ma; [*Liebrand et al.*, 2017; *Pälike et al.*, 2006]). The BAEs coincide with the latest part of the early Oligocene cooling trend, suggesting that hyperstratification in the South Atlantic Ocean occurred during relatively colder conditions globally. In addition to climatic boundary conditions, tectonic processes, such as the opening

of ocean gateways, may have affected the timing of the BAEs on multi-My time scales [*Kelly et al.*, 2003; *Peleo-Alampay et al.*, 1999].

6. Conclusions

We identify strong ~2.4-My and 405-ky eccentricity pacing of *Braarudosphaera* acme events at Walvis Ridge Site 1264, which broadly correlate to other similar events reported at mid-latitude South Atlantic sites. We interpret the underlying mechanism of the acmes to be insolation-controlled (predominantly precession) latitudinal migrations of atmospheric and oceanic fronts, and the effect this has on either the hydrological cycle and oceanic and circum-Atlantic rainfall and runoff (i.e., the Monsoon Hypothesis), or the amount of eddies derived from the proto-Benguela Current and/or the Agulhas retroflection (i.e., the Eddy Hypothesis). Both mechanisms link astronomical forcing of the mid-Oligocene climate system to regional or local pycnocline (thermocline) shallowing, surface ocean hyperstratification, and to the unusual increase in calcification and export productivity of the prymnesiophyte alga *Braarudosphaera*. We suggest that the BAEs concur with a ~2.4-My eccentricity minimum when the amplitude of precession is reduced (and the ~1.2-My obliquity cycle has a maximum amplitude), because winter monsoon conditions were limiting *Braarudosphaera* acmes during times with relatively higher amplitude precession cycles (i.e., ~2.4-My eccentricity maxima), through insufficient oceanic rainfall and/or too much surface ocean mixing (Monsoon Hypothesis), or through limited formation of proto-Benguela upwelling eddies and/or limited number of Agulhas rings making it into the South Atlantic (Eddy Hypothesis). In these hypotheses, the acmes were annually amplified during the relatively wetter summer monsoons, or when most eddies were shed, as is suggested by laminae preserved in some *Braarudosphaera* oozes. Hyperstratification and the development of a shallow pycnocline/thermocline that may have served as a virtual seafloor, is supported

by modern biogeographical distribution of *Braarudosphaera*, and by its alternating life cycle stages. The likely need of *Braarudosphaera* for a real or virtual seafloor to prevent it from sinking during its non-motile calcifying life cycle stage would reconcile the contrasting distribution patterns of *Braarudosphaera* in the modern ocean (shallow water coastal settings) compared to their relatively brief and expanded oceanic distribution in the past. However, further constraints on *Braarudosphaera*'s life cycle are needed to be certain about a potential benthic resting stage. Until such data becomes available, we tentatively interpret *Braarudosphaera* as a hyperstratification indicator – a potential finding that may apply to other regions in the global ocean that have *Braarudosphaera*-rich deposits.

Acknowledgements

We are grateful for the help, advice, and support we received from: Richard Pearce and Wilma Wessels when taking micrographs, Linda Hinnov by providing her evolutive analysis MATLAB script, Tom Chalk with plotting the sea surface salinity and nutrient data, and Arnold van Dijk with bulk stable isotope mass spectrometry. We thank Clay Kelly for providing samples and Kyoko Hagino for commenting on an early version of this manuscript. We thank Jan Backman, Kyoko Hagino, Clay Kelly, and Alyssa Peleo-Alampay for their constructive reviews, and Ellen Thomas for the editorial handling of this manuscript. We used samples provided by the Ocean Drilling Program, sponsored by the US National Science Foundation and participating countries under the management of the Joint Oceanographic Institutions. We are greatly indebted to the scientists and supporting staff of ODP Leg 208. This research has been made possible through funding of NWO grant 865.10.001 (Utrecht), NERC grant NE/K014137/1 (Southampton) and European Research Council Grant 617462 (Bremen). All data presented in this paper are available online (www.pangaea.de). For the previously published benthic stable isotope records, $CaCO_3$ estimate record, and size fraction

records follow this link: https://doi.pangaea.de/10.1594/PANGAEA.862589. For the newly generated water content record, bulk stable isotope records, and calcareous nannofossil abundance records follow this link: https://doi.pangaea.de/10.1594/PANGAEA.878110.

References

Agnini, C., E. Fornaciari, I. Raffi, R. Catanzariti, H. Pälike, J. Backman, and D. Rio (2014), Biozonation and biochronology of Paleogene calcareous nannofossils from low and middle latitudes, Newsl Stratigr, 47(2), 131-181, doi: 10.1127/0078-0421/2014/0042.

Arhan, M., H. Mercier, and J. R. E. Lutjeharms (1999), The disparate evolution of three Agulhas rings in the South Atlantic Ocean, J Geophys Res-Oceans, 104(C9), 20987-21005, doi: Doi 10.1029/1998jc900047.

Backman, J., and N. J. Shackleton (1983), Quantitative Biochronology of Pliocene and Early Pleistocene Calcareous Nannofossils from the Atlantic, Indian and Pacific Oceans, Marine Micropaleontology, 8(2), 141-170, doi: Doi 10.1016/0377-8398(83)90009-9.

Bard, E., and R. E. M. Rickaby (2009), Migration of the subtropical front as a modulator of glacial climate, Nature, 460(7253), 380-U393, doi: 10.1038/nature08189.

Bartol, M., J. Pavšič, M. Dobnikar, and S. M. Bernasconi (2008), Unusual *Braarudosphaera bigelowii* and *Micrantholithus vesper* enrichment in the Early Miocene sediments from the Slovenian Corridor, a seaway linking the Central Paratethys and the Mediterranean, Palaeogeography, Palaeoclimatology, Palaeoecology, 267, 77 - 88.

Billard, C., and I. Inouye (2004), What is new in coccolithophore biology?, in Coccolithophores – From Molecular Processes to Global Impact, edited by H. R. Thierstein and J. R. Young, pp. 1-29, Springer, Berlin.

Boeckel, B., and K.-H. Baumann (2004), Distribution of coccoliths in surface sediments of the south-eastern South Atlantic Ocean: ecology, preservation and carbonate contribution, Marine Micropaleontology, 51, 301 - 320.

Bolli, H. M., et al. (1978), Initial Reports: Leg 40*Rep.*, U. S. Government Printing Office, Washington D. C.

Bolton, C. T., H. M. Stoll, and A. Mendez-Vicente (2012), Vital effects in coccolith calcite: Cenozoic climate-pCO(2) drove the diversity of carbon acquisition strategies in coccolithophores?, Paleoceanography, 27, doi: Artn Pa4204 10.1029/2012pa002339.

Bosmans, J. H. C., F. J. Hilgen, E. Tuenter, and L. J. Lourens (2015a), Obliquity forcing of low-latitude climate, Clim Past, 11(10), 1335-1346, doi: 10.5194/cp-11-1335-2015.

Bosmans, J. H. C., S. S. Drijfhout, E. Tuenter, F. J. Hilgen, and L. J. Lourens (2015b), Response of the North African summer monsoon to precession and obliquity forcings in the EC-Earth GCM, Clim Dynam, 44(1-2), 279-297, doi: 10.1007/s00382-014-2260-z.

Bosmans, J. H. C., S. S. Drijfhout, E. Tuenter, F. J. Hilgen, L. J. Lourens, and E. J. Rohling (2015c), Precession and obliquity forcing of the freshwater budget over the Mediterranean, Quaternary Sci Rev, 123, 16-30, doi: 10.1016/j.quascirev.2015.06.008.

Bowles, J. (2006), Data report: revised magnetostratigraphy and magnetic mineralogy of sediments from Walvis Ridge, Leg 208*Rep.*, Ocean Drilling Program, College Station, TX.

Bown, P. R. (2005a), Calcareous nannoplankton evolution: a tale of two oceans, Micropaleontology, 51(4), 299-308, doi: DOI 10.2113/gsmicropal.51.4.299.

Bown, P. R. (2005b), Selective calcareous nannoplankton survivorship at the Cretaceous-Tertiary boundary, Geology, 33(8), 653-656, doi: 10.1130/G21566.

Bown, P. R. (2010), Calcareous nannofossils from the Paleocene/Eocene Thermal Maximum interval of southern Tanzania (TDP Site 14), Journal of Nannoplankton Research, 31(1), 11-38.

Bown, P. R., and J. R. Young (1998), Techniques, in Calcareous Nannoplankton Biostratigraphy, edited by P. R. Bown, pp. 16-28, Kluwer Academic Publishers, London.

Bukry, D. (1974), Coccoliths as paleosalinity indicators - Evidence from the Black Sea, The American Association of Petroleum Geologists, Tulsa, Oklahoma.

Bukry, D. (1978a), Cenozoic silicoflagellate and coccolith stratigraphy, southeastern Atlantic Ocean, Deep Sea Drilling Project Leg 40*Rep.*, U. S. Governmental Printing Office, Washington D. C.

Bukry, D. (1978b), Biostratigraphy of Cenozoic marine sediment by calcareous nannofossils Micropaleontology, 24(1), 44-60, doi: 10.2307/1485419.

Bukry, D. (1981), Cenozoic coccoliths from the Deep Sea Drilling Project, SEPM Special Publication, 32, 335-353.

Bybell, L., and S. Gartner (1972), Provincialism among mid-Eocene calcareous nannofossils, Micropaleontology, 18(3), 319-336.

Chelton, D. B., M. G. Schlax, and R. M. Samelson (2011), Global observations of nonlinear mesoscale eddies, Prog Oceanogr, 91(2), 167-216, doi: 10.1016/j.pocean.2011.01.002.

Cunha, A. A. S., and S. Shimabukuro (1997), *Braarudosphaera* blooms and anomalous enrichments of *Nannoconus*: evidence from the Turonian South Atlantic, Santos Basin, Brazil Journal of Nannoplankton Research, 19(1), 51 - 55.

Diester-Haass, L. (1988), Sea level changes, carbonate dissolution and history of the Benguela Current in the Oligocene-Miocene off southwest Africa (DSDP Site 362, Leg 40), Marine Geology, 79, 213-242, doi: https://doi.org/10.1016/0025-3227(88)90040-0.

Diester-Haass, L., P. A. Meyers, and P. Rothe (1990), Miocene history of the Benguela Current and Antarctic ice volumes: Evidence from rhythmic sedimentation and current growth across the Walvis Ridge (Deep Sea Drilling Project Sites 362 and 532), Paleoceanography, 5(5), 685-707, doi: 10.1029/PA005i005p00685.

Donohoe, A., J. Marshall, D. Ferreira, and D. Mcgee (2013), The Relationship between ITCZ Location and Cross-Equatorial Atmospheric Heat Transport: From the Seasonal Cycle to the Last Glacial Maximum, J Climate, 26(11), 3597-3618, doi: 10.1175/Jcli-D-12-00467.1.

Fischer, A. G., S. Honjo, and R. E. Garrison (1967), Electron micrographs of limestones and their nannofossils, Princeton Monogr. Geol. Paleontol., Mon., 1, 1-141.

Gartner, S. (1996), Calcareous nannofossils at the Cretaceous-Tertiary boundary, in Cretaceous-Tertiary mass extinctions: Biotic and environmental changes, edited by N. MacLeod and G. Keller, pp. 27-47, W. W. Norton, New York.

Garzoli, S. L., P. L. Richardson, C. M. Duncombe Rae, D. M. Fratantoni, G. J. Goni, and A. J. Roubicek (1999), Three Agulhas rings observed during the Benguela Current experiment, J Geophys Res-Oceans, 104(C9), 20971-20985, doi: Doi 10.1029/1999jc900060.

Ghil, M., et al. (2002), Advanced spectral methods for climatic time series, Reviews of Geophysics, 40.

Grinsted, A., J. C. Moore, and S. Jevrejeva (2004), Application of the cross wavelet transform and wavelet coherence to geophysical time series, Nonlinear Processes in Geophysics, 11, 561-566.

Hagino, K. (1997), Distribution of living coccolithophores in the western Pacific Ocean off the coast of northeast Japan Fossils, 63, 1-19.

Hagino, K., R. Onuma, M. Kawachi, and T. Horiguchi (2013), Discovery of an endosymbiotic nitrogen-fixing cyanobacterium UCYN-A in *Braarudosphaera bigelowii* (Prymnesiophyceae), Plos one, 8(12).

Hagino, K., N. Tomioka, J. R. Young, Y. Takano, R. Onuma, and T. Horiguchi (2016), Extracellular calcification of *Braarudosphaera bigelowii* deduced from electron microscopic observations of cell surface structure and elemental composition of pentaliths, Marine Micropaleontology, 125, 85-94, doi: 10.1016/j.marmicro.2016.04.002.

Herbette, S., Y. Morel, and M. Arhan (2004), Subduction of a surface vortex under an outcropping front, J Phys Oceanogr, 34(7), 1610-1627, doi: Doi 10.1175/1520-0485(2004)034<1610:Soasvu>2.0.Co;2.

Hermoso, M., T. J. Horner, F. Minoletti, and R. E. M. Rickaby (2014), Constraints on the vital effect in coccolithophore and dinoflagellate calcite by oxygen isotopic modification of seawater, Geochim Cosmochim Ac, 141, 612-627, doi: 10.1016/j.gca.2014.05.002.

Hsü, K. J., et al. (1984), Initial Report: Leg 73*Rep.*, U. S. Goverment Printing Office, Washington D. C. .

Hyeong, K., J. Kuroda, I. Seo, and P. A. Wilson (2016), Response of the Pacific inter-tropical convergence zone to global cooling and initiation of Antarctic glaciation across the Eocene Oligocene Transition, Sci Rep-Uk, 6, doi: ARTN 30647 10.1038/srep30647.

Kelly, D. C., R. D. Norris, and J. C. Zachos (2003), Deciphering the paleoceanographic significance of Early Oligocene *Braarudosphaera* chalks in the South Atlantic, Marine Micropaleontology, 49, 49 - 63.

Konno, S., N. Harada, H. Narita, and R. W. Jordan (2007), Living *Braarudosphaera bigelowii* (Gran & Braarud) Deflandre in the Bering Sea, Journal of Nannoplankton Research, 29(2), 78-87.

Lamolda, M. A., M. C. Melinte, and K. Kaiho (2005), Nannofloral extinction and survivorship across the K/T boundary at Caravaca, southeastern Spain, Palaeogeogr Palaeocl, 224(1-3), 27-52, doi: 10.1016/j.palaeo.2005.03.030.

Laskar, J., M. Gastineau, J. B. Delisle, A. Farres, and A. Fienga (2011), Strong chaos induced by close encounters with Ceres and Vesta, Astron Astrophys, 532.

Laskar, J., P. Robutel, F. Joutel, M. Gastineau, A. C. M. Correia, and B. Levrard (2004), A long-term numerical solution for the insolation quantities of the Earth, Astron Astrophys, 428(1), 261-285.

Lehahn, Y., F. d'Ovidio, M. Levy, Y. Amitai, and E. Heifetz (2011), Long range transport of a quasi isolated chlorophyll patch by an Agulhas ring, Geophysical Research Letters, 38, doi: Artn L16610 10.1029/2011gl048588.

Liebrand, D., L. J. Lourens, D. A. Hodell, B. de Boer, R. S. W. van de Wal, and H. Palike (2011), Antarctic ice sheet and oceanographic response to eccentricity forcing during the early Miocene, Clim Past, 7(3), 869-880, doi: 10.5194/cp-7-869-2011.

Liebrand, D., et al. (2016), Cyclostratigraphy and eccentricity tuning of the early Oligocene through early Miocene (30.1–17.1 Ma): *Cibicides mundulus* stable oxygen and carbon isotope records from Walvis Ridge Site 1264, Earth and Planetary Science Letters, 450, 392-405, doi: 10.1016/j.epsl.2016.06.007.

Liebrand, D., et al. (2017), Evolution of the early Antarctic ice ages, Proceedings of the National Academy of Sciences of the United States of America, 114(15), 3867-3872, doi: 10.1073/pnas.1615440114.

Liu, Z., et al. (2009), Transient simulation of last deglaciation with a new mechanism for Bølling-Allerød Warming, Science, 325(5938), 310-314, doi: 10.1126/science.1171041.

Martini, E. (1967), Nannoplankton und Umlagerungserscheinungen im Persischen Golf und im nördlichen Arabischen Meer, Neus Jahrb Geol Paläont Monatsch, 10, 597-607.

Maxwell, A. E., R. P. von Herzen, J. E. Andrews, R. E. Boyce, E. D. Milow, K. J. Hsu, S. F. Percival, and T. Saito (1970), Initial Reports: Leg 3*Rep.*, National Science Foundation, Washington D. C.

McGillicuddy Jr., D. J. (2016), Mechanisms of Physical-Biological-Biogeochemical Interaction at the Oceanic Mesoscale, Annual Review of Marine Science, 8, 125-159, doi: 10.1146/annurev-marine-010814-015606.

Minoletti, F., M. de Rafelis, M. Renard, S. Gardin, and J. Young (2005), Changes in the pelagic fine fraction carbonate sedimentation during the Cretaceous-Paleocene transition: contribution of the separation technique to the study of Bidart section, Palaeogeogr Palaeocl, 216(1-2), 119-137, doi: 10.1016/j.palaeo.2004.10.006.

Mohtadi, M., M. Prange, and S. Steinke (2016), Palaeoclimatic insights into forcing and response of monsoon rainfall, Nature, 533(7602), 191-199, doi: 10.1038/nature17450.

Moore, T. C., et al. (1984), Initial Reports: Leg 74*Rep.*, U. S. Government Printing Office, Washington D. C.

Noël, D., and M. Melguen (1978), Nannofacies of Cape Basin and Walvis Ridge Sediments, Lower Cretaceous to Pliocene (Leg 40)*Rep.*, U. S. Government Printing Office, Washinton D. C.

O'Connor, J. M., and R. A. Duncan (1990), Evolution of the Walvis Ridge-Rio Grande Rise hot spot system: Implication for African and South American plate motions over plumes, Journal of Geophysical Research, 95(B11), 17475 - 17502.

Otto-Bliesner, B. L., J. M. Russell, P. U. Clark, Z. Y. Liu, J. T. Overpeck, B. Konecky, P. deMenocal, S. E. Nicholson, F. He, and Z. Y. Lu (2014), Coherent changes of southeastern equatorial and northern African rainfall during the last deglaciation, Science, 346(6214), 1223-1227, doi: 10.1126/science.1259531.

Paillard, D., L. Labeyrie, and P. Yiou (1996), AnalySeries, Macintosh program performs time-series analysis, EOS Transactions AGU, 77(39), 379.

Pälike, H., R. D. Norris, J. O. Herrle, P. A. Wilson, H. K. Coxall, C. H. Lear, N. J. Shackleton, A. K. Tripati, and B. S. Wade (2006), The heartbeat of the oligocene climate system, Science, 314(5807), 1894-1898, doi: 10.1126/science.1133822.

Parker, M. E., M. Clark, and S. W. Wise (1985), Calcareous nannofossils of Deep Sea Drilling Project Sites 558 and 563, North Atlantic Ocean: Biostratigraphy and the distribution of Oligocene braarudosphaerids*Rep.*, Washington.

Peeters, F. J. C., R. Acheson, G. J. A. Brummer, W. P. M. de Ruijter, R. R. Schneider, G. M. Ganssen, E. Ufkes, and D. Kroon (2004), Vigorous exchange between the Indian and Atlantic oceans at the end of the past five glacial periods, Nature, 430(7000), 661-665, doi: 10.1038/nature02785.

Pegliasco, C., A. Chaigneau, and R. Morrow (2015), Main eddy vertical structures observed in the four major Eastern Boundary Upwelling Systems, J Geophys Res-Oceans, 120(9), 6008-6033, doi: 10.1002/2015jc010950.

Peleo-Alampay, A. M., G. A. Mead, and W. Wei (1999), Unusual Oligocene *Braarudosphaera*-rich layer of the South Atlantic and their palaeoceanographic implications, Journal of Nannoplankton Research, 21(1), 17 - 26.

Proto Decima, F., F. Medizza, and L. Todesco (1978), Southeastern Atlantic Leg 40 calcareous nannofossils*Rep.*, U. S. Government Printing Office, Washington D. C. .

Raffi, I., C. Ricci, A. Garzarella, M. Brandano, I. Cornacchia, and L. Tomassetti (2016), Calcareous nannofossils as a dating tool in shallow marine environment: an example from an upper Paleogene carbonate platform succession in the Mediterranean, Newsl Stratigr, 49(3), 481-495, doi: 10.1127/nos/2016/0328.

Reichart, G. J., H. Brinkhuis, F. Huiskamp, and W. J. Zachariasse (2004), Hyperstratification following glacial overturning events in the northern Arabian Sea, Paleoceanography, 19(2), doi: Artn Pa2013 10.1029/2003pa000900.

Roth, P. H. (1974), Calcareous nannofossils from the northwestern Indian Ocean, Leg 24, Deep Sea Drilling Project*Rep.*, U.S. Governmental Printing Office, Washington.

Schouten, M. W., W. P. M. de Ruijter, P. J. van Leeuwen, and J. R. E. Lutjeharms (2000), Translation, decay and splitting of Agulhas rings in the southeastern Atlantic Ocean, J Geophys Res-Oceans, 105(C9), 21913-21925, doi: Doi 10.1029/1999jc000046.

Siesser, W. G., T. J. Bralower, and E. H. De Carlo (1992), Mid-Teriary *Braarudosphaera*-rich sediments on the Exmouth Plateau*Rep.*, Ocean Drilling Program, College Station, Tx.

Souza, J. M. A. C., C. D. Montegut, C. Cabanes, and P. Klein (2011), Estimation of the Agulhas ring impacts on meridional heat fluxes and transport using ARGO floats and satellite data, Geophysical Research Letters, 38, doi: Artn L21602 10.1029/2011gl049359.

Stoll, H. M., and P. Ziveri (2004), Coccolithophorid-based geochemical paleoproxies, Coccolithophores: From Molecular Processes to Global Impact, 529-562.

Švábenická, L. (1999), *Braarudosphaera*-rich sediments in the Turonian of the Bohemian Cretaceous Basin, Czech Republic, Cretaceous Research, 20, 773 - 782.

Takano, Y., K. Hagino, Y. Tanaka, T. Horiguchi, and H. Okada (2006), Phylogenetic affinities of an enigmatic nannoplankton, *Braarudosphaera bigelowii* based on SSU rDNA sequences, Marine Micropaleontology, 60, 145 - 156.

Takayama, T. (1972), A note on the distribution of *Braarudosphaera bigelowi* (Gran and Braarud) Deflandre in the bottom sediments of Senday Bay, Japan, Trans. Proc. Palaeont. Soc. Japan, 87, 429-435.

Tanaka, Y. (1991), Calcareous nannoplankton thanatocoenoses in surface sediments from seas around Japan*Rep.*, 127-198 pp, Tohoky University.

Thompson, A. W., R. A. Foster, A. Krupke, B. J. Carter, N. Musat, D. Vaulot, M. M. M. Kuypers, and J. P. Zehr (2012), Unicellular cyanobacterium symbiotic with a single-celled eukaryotic alga, Science, 337, 1546 - 1550.

Vandenberghe, N., F. J. Hilgen, and R. P. Speijer (2012), Chapter 28: The Paleogene Period, in The Geologic Time Scale 2012, edited by F. M. Gradstein, J. G. Ogg, M. Schmitz and G. M. Ogg, Elsevier, Oxford, Amsterdam, Waltham.

Villar, E., et al. (2015), Environmental characteristics of Agulhas rings affect interocean plankton transport, Science, 348(6237), doi: ARTN 1261447 10.1126/science.1261447.

Wang, Y., M. J. Olascoaga, and F. J. Beron-Vera (2015), Coherent water transport across the South Atlantic, Geophysical Research Letters, 42(10), 4072-4079, doi: 10.1002/2015gl064089.

Young, J. R., M. Geisen, L. Cros, A. Kleijne, I. Probert, and J. B. Ostergaard (2003), A guide to extant coccolithophore taxonomy, Journal of Nannoplankton Research(Special Issue 1), 1-132.

Zachos, J. C., D. Kroon, P. Blum, and e. al. (2004), Initial Reports: Leg 208*Rep. Volume 208*, Ocean Drilling Program.

Zeeden, C., F. J. Hilgen, S. K. Husing, and L. J. Lourens (2014), The Miocene astronomical time scale 9-12 Ma: New constraints on tidal dissipation and their implications for paleoclimatic investigations, Paleoceanography, 29(4), 296-307, doi: 10.1002/2014pa002615.

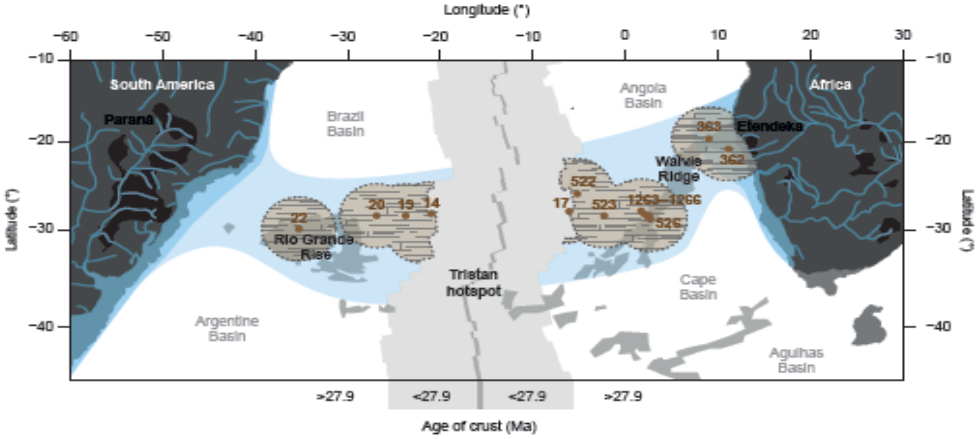

Figure 1. Geographic extent of *Braarudosphaera*-rich layers. Modern geography of the South Atlantic Ocean with the locations of DSDP and ODP drill sites (brown areas with chalk-pattern) wherefrom mid-Oligocene *Braarudosphaera*-rich layers have been recovered. For South Atlantic Ocean sites information from the relevant DSDP and ODP site reports is recompiled. For a global compilation of Oligocene strata with and without *Braarudosphaera* recovered from DSDP and ODP sites (until 1999) we refer to *Peleo-Alampay et al.*, [1999]. Blue lines on continents represent modern-day rivers that may have delivered fresh waters to the South Atlantic surface ocean. Light blue areas project the potential mid-Oligocene extent of seasonally recurrent surface-ocean stratification caused by increased precipitation over the sea, possibly aided by increased continental runoff closer to the coasts, indicated by a darker blue. According to the eccentricity-tuned age model [*Liebrand et al.*, 2016], the *Braarudosphaera* oozes are present on oceanic crust ≥27.9 Ma. This figure is an adaptation of figures from refs: [*Kelly et al.*, 2003; *O'Connor and Duncan*, 1990; *Parker et al.*, 1985; *Peleo-Alampay et al.*, 1999], and combines geographic information and anomaly profiles of www.odsn.de and www.serg.unicam.it, respectively.

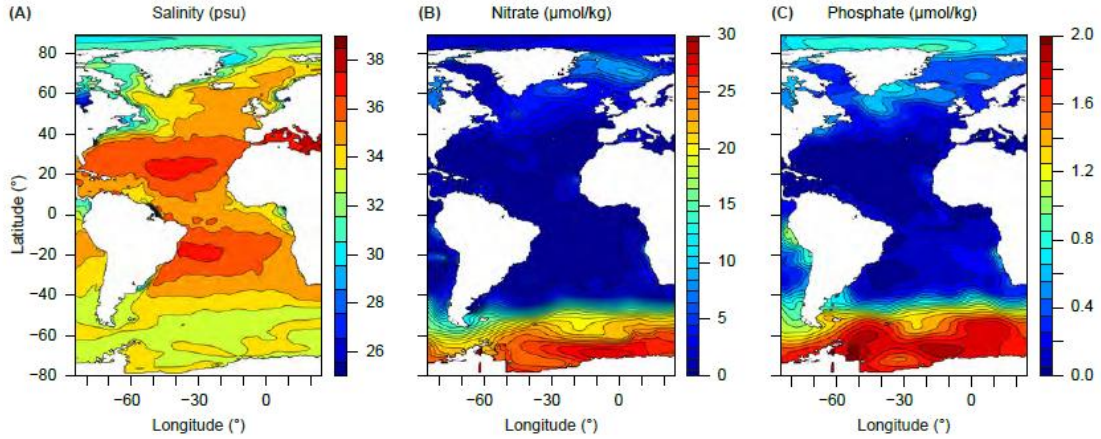

Figure 2. Modern sea-surface salinity, and sea-surface nitrate and phosphate concentrations. (A) Sea-surface salinity, which show relatively hypersaline conditions in the modern South Atlantic Ocean. **(B)** Sea-surface nitrate concentrations, and **(C)** sea-surface phosphate concentration, which show relatively oligotrophic conditions in the modern South Atlantic Ocean. Data taken from www.eWOCE.org.

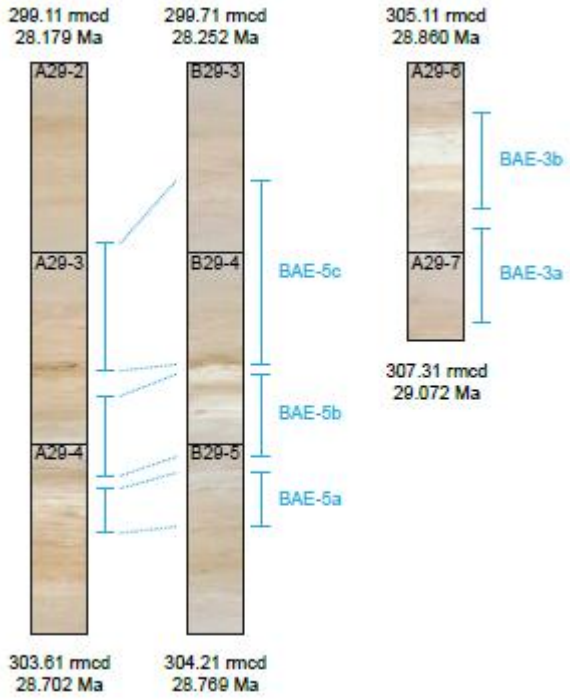

Figure 3. Core photographs of *Braarudosphaera* oozes. On-splice and off-splice examples of the lithologic expression of *Braarudosphaera* Acme Events (BAEs) 3, 5a and 5b at Site 1264. Strong color variability between and within the acmes can be observed, suggesting higher-frequency precession and/or obliquity forcing. The color contrast of the images is enhanced.

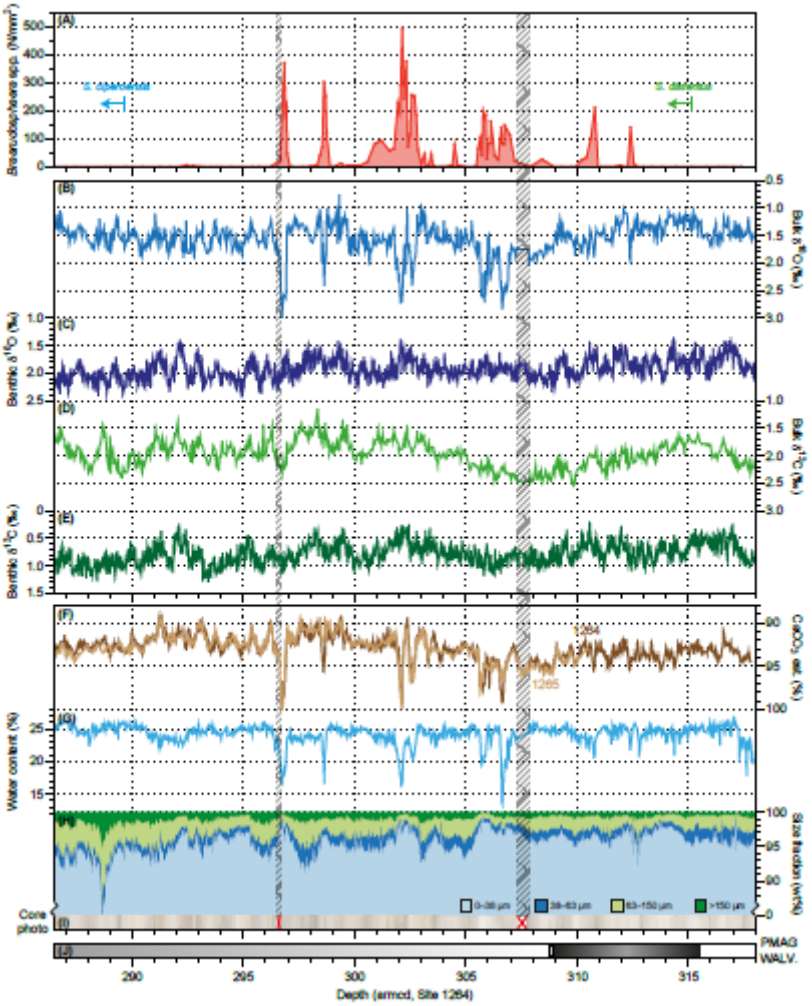

Figure 4. Stratigraphy across the *Braarudosphaera* oozes. The data records are presented against stratigraphic depth (armcd = adjusted revised meters composite depth, see [*Liebrand et al.*, 2016]). **(A)** *Braarudosphaera* spp. abundances. The biohorizons Base *Sphenolithus ciperoensis* and Base *Sphenolithus distentus* are indicated. **(B–E)** Stable isotope records. **(B)** Bulk and **(C)** benthic foraminiferal (*Cibicides mundulus*) $\delta^{18}O$ records. **(D)** Bulk and **(E)** benthic foraminiferal (*Cibicides mundulus*) $\delta^{13}C$ records. **(F–I)** Lithological records. **(F)** $CaCO_3$ estimates for Sites 1264 (dark brown) and 1265 (light brown). Percentages refer to dry weights (i.e., after freeze-drying). **(G)** Water content of samples. Percentages refer to total sample weights (i.e., before freeze-drying). **(H)** Size fraction records from Site 1264. Percentages as in panel (F). **(I)** Core photographs from Site 1264. Apparent cyclicity results from uneven lighting conditions when the photographs were taken. Red crosses and shaded area indicate short recovery gaps at Site 1264. These gaps are covered by data from nearby Site 1265 (both XRF and isotopes). **(J)** Magnetostratigraphy from Site 1266 transposed to

Site 1264 depth [*Liebrand et al.*, 2016]. The shaded gray areas indicate that the polarity signal is ambiguous in these intervals.

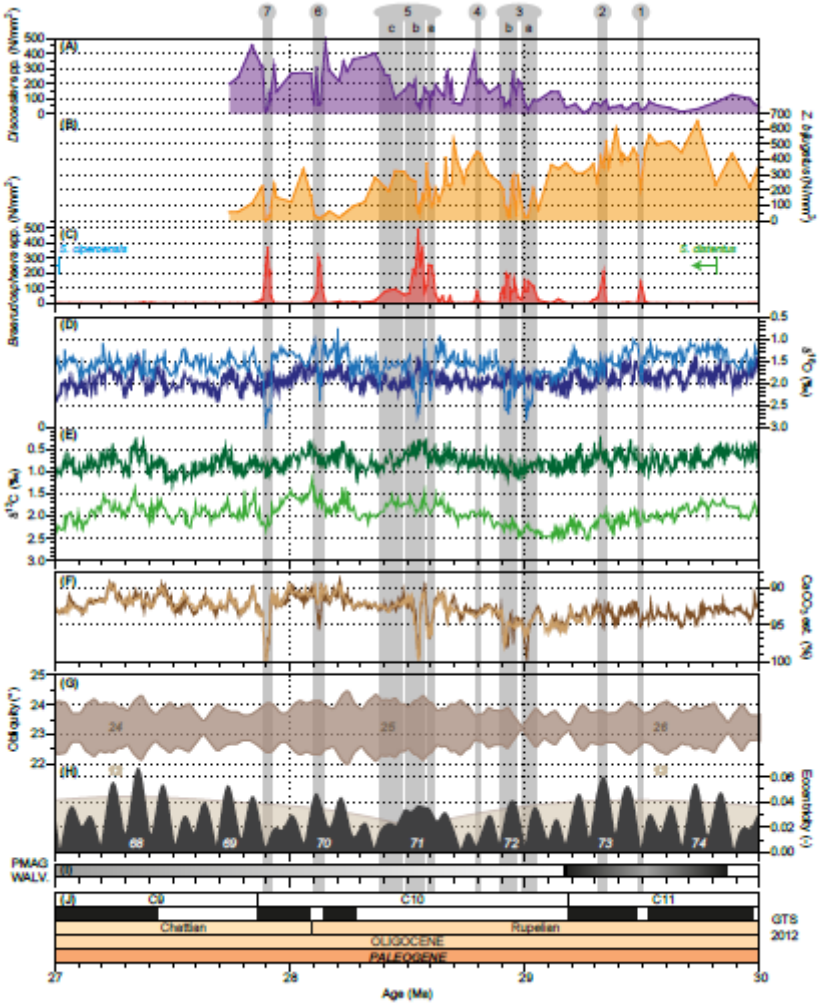

Figure 5. Astrochronology for the mid-Oligocene *Braarudosphaera* acmes. The data records are presented against eccentricity-tuned age [*Liebrand et al.*, 2016].

(A-C) Calcareous nannofossil records. **(A)** *Discoaster* spp. abundances. **(B)** *Zygrhablithus bijugatus* abundances. **(C)** *Braarudosphaera* spp. abundances. Vertical grey bars correspond to the *Braarudosphaera* acmes. The biohorizons Base *Sphenolithus ciperoensis* and Base *Sphenolithus distentus* are indicated. **(D-E)** Stable isotope records. **(D)** Bulk (light blue) and benthic (dark blue) foraminiferal (*Cibicides mundulus*) $\delta^{18}O$ records. **(E)** Bulk (light green) and benthic (dark green) foraminiferal (*Cibicides mundulus*) $\delta^{13}C$ records. **(F)** $CaCO_3$ estimates for Sites 1264 (dark brown) and 1265 (light brown). **(G-H)** Astronomical solutions. **(G)** Earth's obliquity modulation [*Laskar et al.*, 2004]. **(H)** Earth's orbital eccentricity solution (dark grey, La2011_ecc3L, [*Laskar et al.*, 2011]) and its ~2.4-My component (light brown). **(I)** Magnetostratigraphy from Walvis Ridge (WALV). PMAG = paleomagnetism. **(J)** The geologic (magnetic polarity) time scale (GTS2012, [*Vandenberghe et al.*, 2012]).

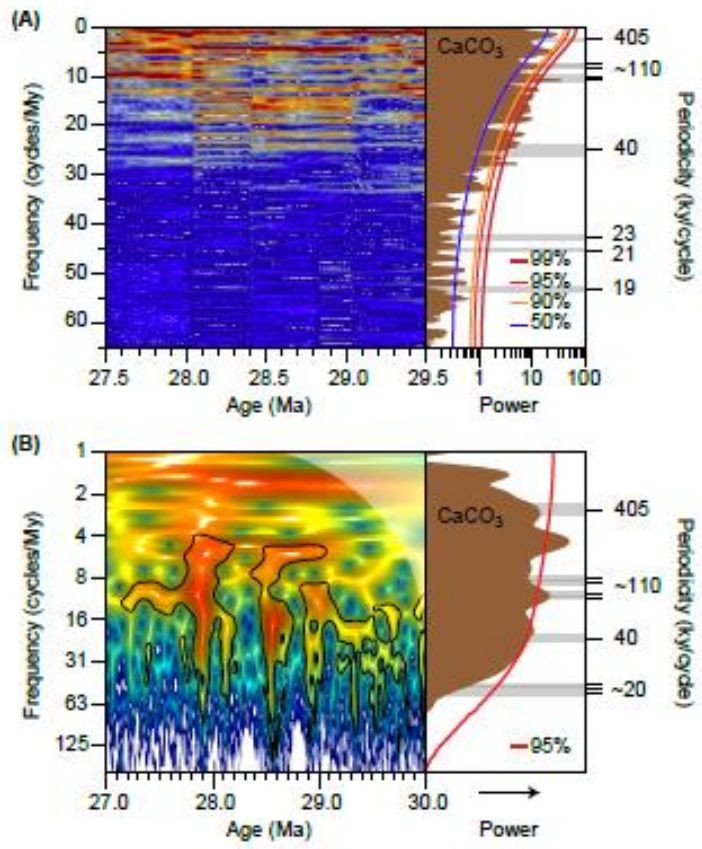

Figure 6. Spectral analyses on carbonate content. (A) Evolutive spectral analysis and singular spectrum analysis on the $CaCO_3$ record using a multi-taper method [*Ghil et al.*, 2002]. **(B)** Wavelet analysis and global spectrum analysis on the $CaCO_3$ record. Black lines on the wavelet analysis and red lines on the spectral analyses represent the 95% confidence level. White shaded area in top right corner represents the 'cone of influence', where edge effects become important [*Grinsted et al.*, 2004]. For both panels: blue colors indicate low spectral power and red colors indicate high spectral power.

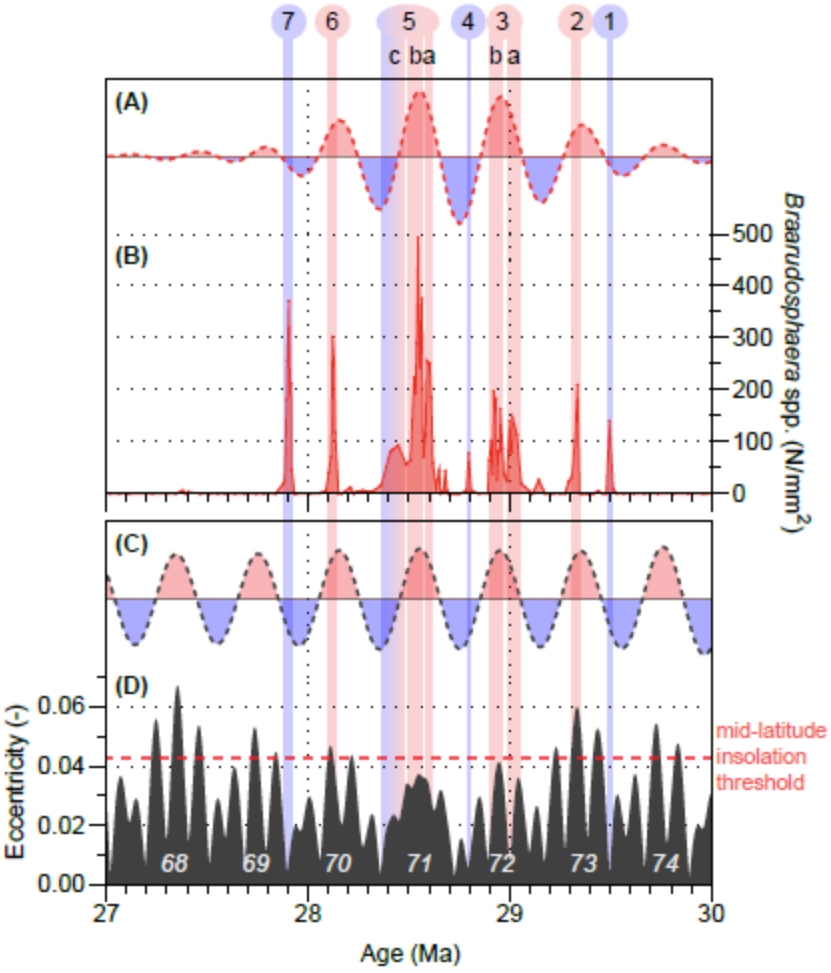

Figure 7. Eccentricity pacing of hyperstratification and *Braarudosphaera* acmes. (A) Gaussian filter of the *Braarudosphaera* spp. abundance record centered around the 405-ky periodicity (i.e., frequency = 2.5, bandwidth = 0.5, [*Paillard et al.*, 1996]). **(B)** *Braarudosphaera* spp. abundance record. **(C)** Gaussian filter of the 405-ky eccentricity periodicity. **(D)** Earth's orbital eccentricity [*Laskar et al.*, 2011]. Vertical red lines correspond to *Braarudosphaera* acmes that occurred during 405-ky and ~110-ky eccentricity maxima. Vertical blue lines show those acmes that correspond to 405-ky and ~110-ky eccentricity minima.

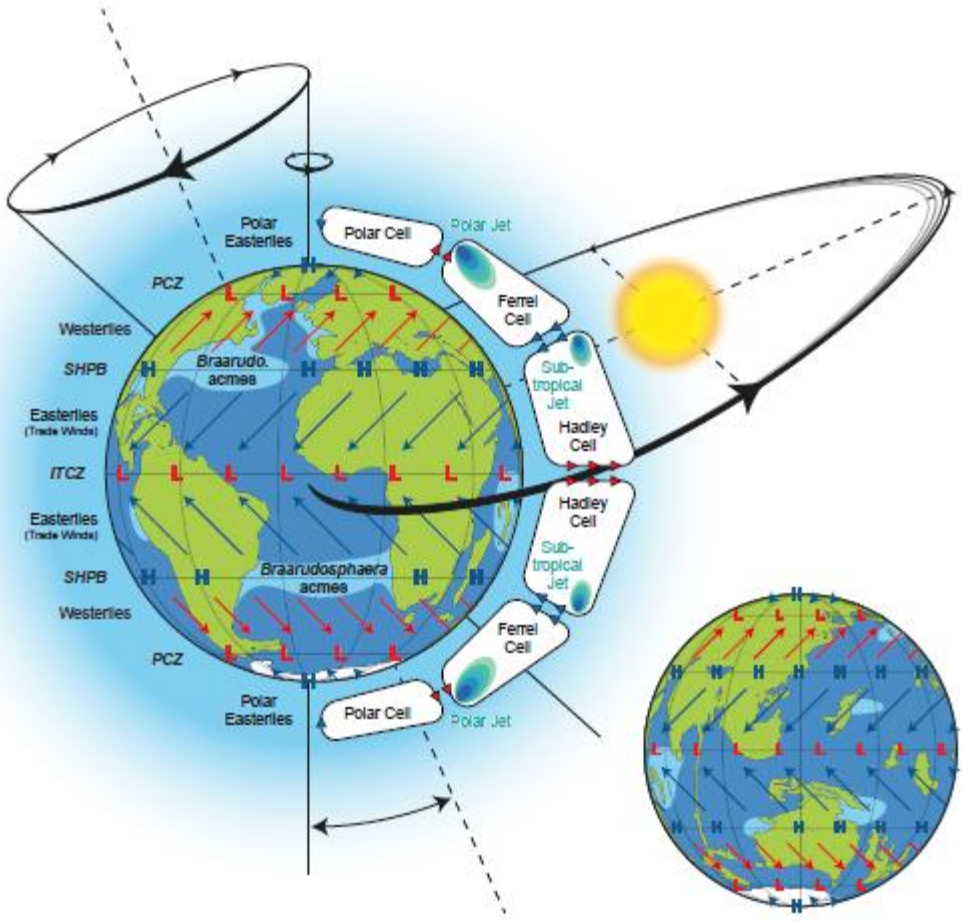

Figure 8. Links between atmospheric circulation, hyperstratification and *Braarudosphaera* acmes. Atmospheric circulation and areal extent of the *Braarudosphaera* acmes drawn on a paleogeographic reconstruction for the mid-Oligocene (~28.5 Ma, www.odsn.de). ITCZ stands for inter-tropical convergence zone. SHPB stands for subtropical high-pressure belt, PCZ stands for polar convergence zone. H = area of generally high air pressure. L = area of generally low air pressure. This figure is based on those by *Parker et al*., [1985] and *Peleo-Alampay et al*., [1999].

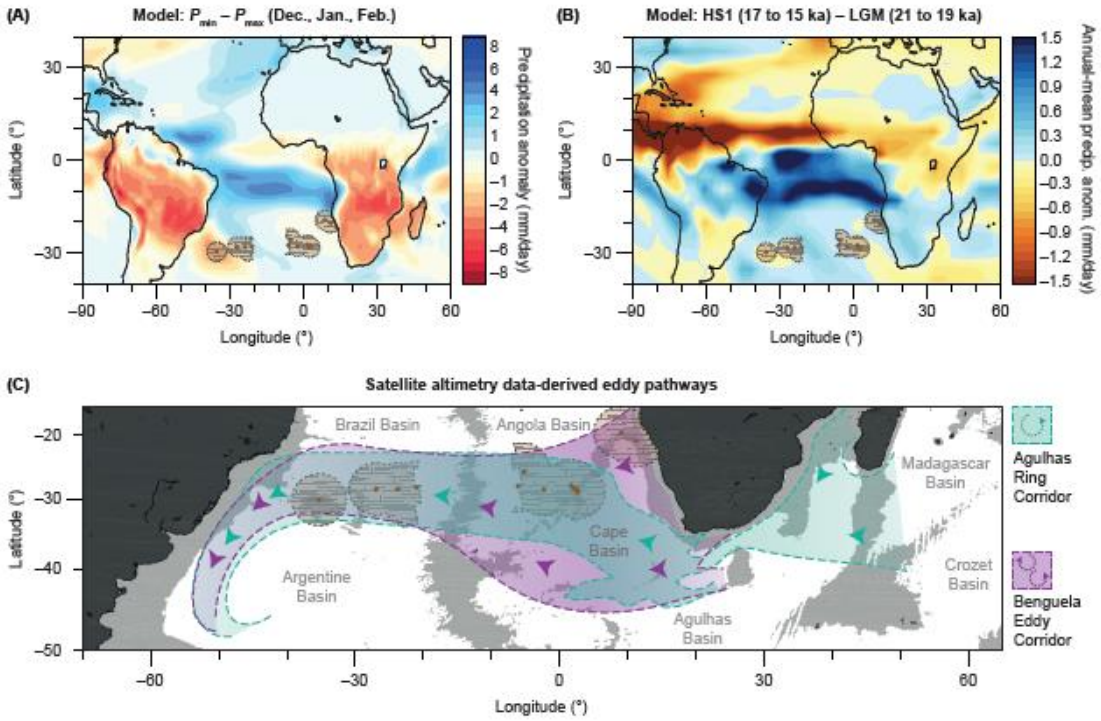

Figure 9. Modeling outputs showing latitudinal rainfall bands that span the South Atlantic Ocean. (A) EC-Earth modeling output shows the influence of precession extremes on precipitation redistribution across the globe using modern day geography [*Bosmans et al.*, 2015a; *Bosmans et al.*, 2015b]. P stands for precession. **(B)** Modeling output of a transient simulation of climate evolution of the past 21 ky using a fully coupled global climate model (i.e., CCSM3) that includes radiative forcing. It shows that during the last glaciation meridional overturning circulation has the largest control on tropical moisture distribution [*Liu et al.*, 2009; *Otto-Bliesner et al.*, 2014]. HS1 stands for Heinrich Stadial 1. LGM stands for Last Glacial Maximum. The relevance of these models to the Oligocene is that they both show a latitudinal rainfall band across the South Atlantic Ocean. Panels A and B are adapted from *Mohtadi et al.*, [2016]. **(C)** Approximate pathways of Benguela Current-derived cyclonic and anticyclonic eddies (purple) and Agulhas rings (teal), which are almost all anticyclonic, in the modern. This panel is loosely based on satellite altimetry data presented in [*Chelton et al.*, 2011; *Pegliasco et al.*, 2015; *Schouten et al.*, 2000; *Souza et al.*, 2011; *Wang et al.*, 2015].

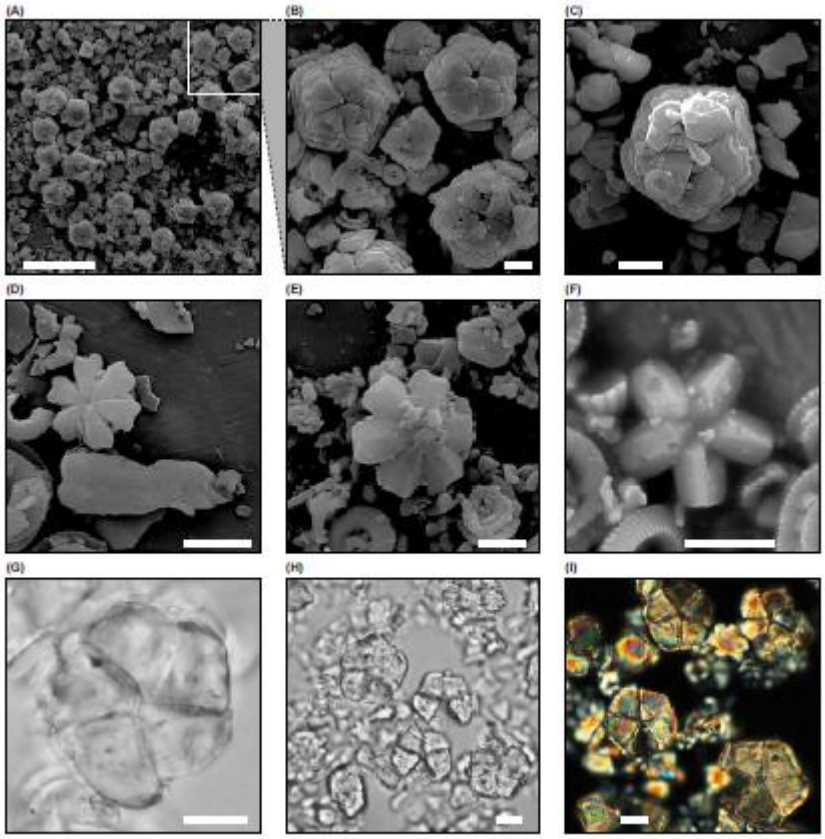

Plate 1. Micrographs of calcareous nannofossils. (A–C) Scanning Electron Microscope (SEM) micrographs of *Braarudosphaera* spp. pentaliths. Specimens show strong overgrowth of calcite and micron-sized crystals and particles. Disintegrated fragments of *Braarudosphaera* can be seen in the background. **(D–F)** SEM micrographs of *Discoaster* specimens show strong calcite overgrowth. **(D)** *Discoaster deflandrei* and *Zygrhablithus bijugatus*, **(E)** *Discoaster deflandrei*. **(F)** *Discoaster* cf. *D. tanii*. **(G–I)** Light microscope micrographs of *Braarudosphaera* spp., **(G, H)** Parallel light. **(I)** Crossed nicols. Horizontal bars in all micrographs are 5 μm, apart from panel (A) where the bar represents 50 μm. Samples ordered with increasing depth/age: **(D, E)** Sample #3553, 301.985 armcd, 28.533 Ma. **(H)** Sample #3558, 302.105 armcd, 28.546 Ma. **(A–C, G, I)** Sample #3566, 302.285 armcd, 28.565 Ma. **(F)** Sample #4042, 314.42 armcd, 29.735 Ma.

Table 1. Durations of *Braarudosphaera* Acme Events. Duration estimates are based on the *Braarudosphaera* spp. abundance record and the eccentricity tuned age model for Site 1264. BAE-3b and 5b consist of three shorter lasting acmes each, which average duration estimates are given in the last column. N/A = not applicable.

Event:	Base age (Ma)	Top age (Ma)	Difference (ky)	Shortest Events (ky)
BAE-1	29.513	29.462	50	N/A
BAE-2	29.347	29.292	55	N/A
BAE-3	29.058	28.899	159	N/A
BAE-3a	29.058	28.985	72	N/A
BAE-3b	28.971	28.899	72	24
BAE-4	28.809	28.786	23	N/A
BAE-5	28.619	28.407	212	N/A
BAE-5a	28.619	28.572	47	N/A
BAE-5b	28.572	28.508	65	22
BAE-5c	28.487	28.407	80	N/A
BAE-6	28.151	28.103	48	N/A
BAE-7	27.919	27.878	41	N/A